Analysis of Brain SPECT Images for the Diagnosis of Alzheimer Disease Using First and Second Order Moments

D. Salas-Gonzalez[1], J.M. Górriz[1], J. Ramírez[1], M. López[1], I. Álvarez[1], F. Segovia[1], and C.G. Puntonet[2]

[1] Dept. of Signal Theory, Networking and Communications, University of Granada, 18071 Granada, Spain
dsalas@ugr.es, gorriz@ugr.es, javierrp@ugr.es
[2] Dept. of Computer Architecture and Computer Technology, University of Granada, 18071, Granada, Spain
carlos@atc.ugr.es

Abstract. This paper presents a computer-aided diagnosis technique for improving the accuracy of the early diagnosis of the Alzheimer type dementia. The proposed methodology is based on the selection of the voxels which present greater overall difference between both modalities (normal and Alzheimer) and also lower dispersion. We measure the dispersion of the intensity values for normals and Alzheimer images by mean of the standard deviation images. The mean value of the intensities of selected voxels is used as feature for different classifiers, including support vector machines with linear kernels, fitting a multivariate normal density to each group and the k-nearest neighbors algorithm. The proposed methodology reaches an accuracy of 92% in the classification task.

1 Introduction

Single Photon Emission Computed Tomography (SPECT) provides three dimensional maps of a pharmaceutical labelled with a gamma ray emitting radionuclide. The distribution of radionuclide concentrations are estimated from a set of projectional images acquired at many different angles around the patient [1].

Single Photon Emission Computed Tomography imaging techniques employ radioisotopes which decay emitting predominantly a single gamma photon. When the nucleus of a radioisotope disintegrates, a gamma photon is emitted with a random direction which is uniformly distributed in the sphere surrounding the nucleus. If the photon is unimpeded by a collision with electrons or other particle within the body, its trajectory will be a straight line. A physical collimator is required to discriminate the direction of the ray by a photon detector external to the patient.

Brain SPECT imaging has become an important diagnostic and research tool in nuclear medicine. The use of brain imaging as a diagnostic tool in neurodegenerative diseases such as Alzheimer type disease (ATD) has been discussed extensively. Many studies have examined the predictive abilities of nuclear imaging

J. Mira et al. (Eds.): IWINAC 2009, Part II, LNCS 5602, pp. 124–133, 2009.
© Springer-Verlag Berlin Heidelberg 2009

with respect to Alzheimer disease and other dementia type illnesses [2, 3, 4, 5, 6]. Clinicians usually evaluate these images via visual inspection. Statistical classification methods have not been widely used for this task, possibly due to the fact images represent large amounts of data and most imaging studies have relatively few subjects (generally < 100). Despite of that, some works have been published recently [7, 8, 9, 10].

In this work, we study the overall difference between SPECT images of normal subjects and images from Alzheimer type disease patients. Firstly, the set of voxels which present greater distance between both categories is selected. A second criterion is chosen to select voxels based on considering those which present not only greater overall difference between both modalities (normal and Alzheimer) but also present lower dispersion. First and second-order moments of normals and ATD images are calculated to measure the distance and dispersion between images respectively. The classification accuracy using the proposed methodology is 92%. The results outperform the accuracy rate obtained in [11], in which, using voxels as features, an accuracy rate of 84.8% and 89.9% was obtained using the nearest mean classifier and Fisher Linear Discriminant ratio respectively.

This work is organised as follows: in Section 2 the classifiers used in this paper are presented: in Section 3, the SPECT image acquisition and preprocessing steps are explained; in Section 4, the approach to select the voxels which will be used in the classification task is explained; in Section 5, we summarize the classification performance obtained applying various classifiers to the selected voxels; lastly, the conclusions are drawn in Section 6.

2 Overview of the Classifiers

The images we work with belong to two different classes: normal and Alzheimer type dementia (ATD). The goal of the classification task is to separate a set of binary labelled training data consisting of, in the general case, N-dimensional patterns $\mathbf{v}_i$ and class labels y_i:

$$(\mathbf{v}_1, y_1), (\mathbf{v}_2, y_2), ..., (\mathbf{v}_l, y_l) \in (R^N \times \{\text{Normal}, \text{ATD}\}), \tag{1}$$

so that a classifier is produced which maps an object $\mathbf{v}_i$ to its classification label y_i. This classifier will correctly classify new examples $(\mathbf{v}, \mathbf{y})$.

There are several different procedures to build the classification rule. We utilize the following classifiers in this work [12].

2.1 Multivariate Normal Model: Linear Discriminant Function

We suppose that $\mathbf{v}$ denotes a p-component random vector of observations made on any individual; $\mathbf{v}_0$ denotes a particular observed value of $\mathbf{v}$, and π_1, π_2 denote the two populations involved in the problem. The basic assumption is that $\mathbf{v}$ has different probability distributions in π_1 and π_2. Let the probability density of $\mathbf{v}$ be $f_1(\mathbf{v})$ in π_1, and $f_2(\mathbf{v})$ in π_2. The simplest intuitive argument, termed the

likelihood ratio rule, classifies $\mathbf{v}_0$ as π_1 whenever it has greater probability of coming from π_1 than from π_2. This classification rule can be written as:

$$v \in \pi_1 \text{ if } f_1(\mathbf{v})/f_2(\mathbf{v}) > 1 \qquad v \in \pi_2 \text{ if } f_1(\mathbf{v})/f_2(\mathbf{v}) \leq 1. \tag{2}$$

The most general form of the model is to assume that π_i is a multivariate normal population with mean $\boldsymbol{\mu}_i$ and dispersion matrix $\boldsymbol{\Sigma}_i$ for $i = 1, 2$. Thus $f_i(\mathbf{v}) = (2\pi)^{-p/2}|\boldsymbol{\Sigma}_i|^{-1/2}\exp\{\frac{1}{2}(\mathbf{v}-\boldsymbol{\mu}_i)'\boldsymbol{\Sigma}_i^{-1}(\mathbf{v}-\boldsymbol{\mu}_i)\}$, so that we obtain

$$\begin{aligned} f_1(\mathbf{v})/f_2(\mathbf{v}) = |\boldsymbol{\Sigma}_2|^{1/2}|\boldsymbol{\Sigma}_1|^{-1/2}\exp[-\frac{1}{2}\{v'(\boldsymbol{\Sigma}_1^{-1}-\boldsymbol{\Sigma}_2^{-1})\mathbf{v} - \\ 2\mathbf{v}'(\boldsymbol{\Sigma}_1^{-1}\boldsymbol{\mu}_1 - \boldsymbol{\Sigma}_2^{-1}\boldsymbol{\mu}_2) + \boldsymbol{\mu}_1'\boldsymbol{\Sigma}_1^{-1}\boldsymbol{\mu}_1 - \boldsymbol{\mu}_2'\boldsymbol{\Sigma}_2^{-1}\boldsymbol{\mu}_2\}] \end{aligned} \tag{3}$$

The presence of two different population dispersion matrices renders difficult the testing of hypothesis about the population mean vectors, therefore, the assumption $\boldsymbol{\Sigma}_1 = \boldsymbol{\Sigma}_2 = \boldsymbol{\Sigma}$ is a reasonable one in many practical situations. The practical benefits of making this assumption are that the discriminant function and allocation rule become very indeed. If $\boldsymbol{\Sigma}_1 = \boldsymbol{\Sigma}_2 = \boldsymbol{\Sigma}$, then

$$f_i(\mathbf{v}) = (2\pi)^{-p/2}|\boldsymbol{\Sigma}|^{-1/2}\exp\{-\frac{1}{2}(\mathbf{v}-\boldsymbol{\mu}_i)'\boldsymbol{\Sigma}^{-1}(\mathbf{v}-\boldsymbol{\mu}_i)\} \tag{4}$$

so that the classification rule reduces to:

Allocate $\mathbf{v}$ to π_1 if $L(\mathbf{v}) > 0$, and otherwise to π_2, where $L(\mathbf{v}) = (\mu_1 - \mu_2)'\Sigma^{-1}\{\mathbf{v} - \frac{1}{2}(\mu_1+\mu_2)\}$. No quadratic terms now exist in the discriminant function $L(\mathbf{v})$, which is therefore called the linear discriminant function.

In any practical application, the parameters $\mu_\mathbf{1}$, $\mu_\mathbf{2}$, $\boldsymbol{\Sigma_1}$ and $\boldsymbol{\Sigma_2}$ are not known. Given two training sets, $\mathbf{v}_1^{(1)}, ..., \mathbf{v}_{n_1}^{(1)}$ from π_1, and $\mathbf{v}_1^{(2)}, ..., \mathbf{v}_{n_2}^{(2)}$ from π_2 we can estimate these parameters by:

$$\boldsymbol{\mu}_1 = \frac{1}{n_1}\sum_{i=1}^{n_1}\mathbf{v}_i^{(1)} \tag{5}$$

$$\boldsymbol{\mu}_2 = \frac{1}{n_2}\sum_{i=1}^{n_2}\mathbf{v}_i^{(2)} \tag{6}$$

$$\boldsymbol{\Sigma}_1 = \frac{1}{n_1-1}\sum_{i=1}^{n_1}(\mathbf{v}_i^{(1)}-\boldsymbol{\mu}_1)(\mathbf{v}_i^{(1)}-\boldsymbol{\mu}_1)' \tag{7}$$

$$\boldsymbol{\Sigma}_2 = \frac{1}{n_2-1}\sum_{i=1}^{n_2}(\mathbf{v}_i^{(2)}-\boldsymbol{\mu}_2)(\mathbf{v}_i^{(2)}-\boldsymbol{\mu}_2)' \tag{8}$$

We estimate the pooled covariance matrix:

$$\Sigma = \frac{1}{n_1+n_2-2}\{\sum_{i=1}^{n_1}(\mathbf{v}_i^{(1)}-\boldsymbol{\mu}_1)(\mathbf{v}_i^{(1)}-\boldsymbol{\mu}_1)' + \sum_{i=1}^{n_2}(\mathbf{v}_i^{(2)}-\boldsymbol{\mu}_2)(\mathbf{v}_i^{(2)}-\boldsymbol{\mu}_2)'\} \tag{9}$$

2.2 Mahalanobis Distance

We use Mahalanobis distance with stratified covariance estimates. The Mahalanobis distance differs from Euclidean in that it takes into account the correlations of the data set and is scale-invariant. We allocate $\mathbf{v}$ to π_1 if $\Delta_1 > \Delta_2$, and otherwise to π_2, where Δ_1, Δ_2 are the Mahalanobis distance between $\mathbf{v}$ and π_1, π_2 respectively:

$$\Delta_1^2 = (\mathbf{v} - \pi_1)'\mathbf{\Sigma_1}(\mathbf{v} - \pi_1), \tag{10}$$

$$\Delta_2^2 = (\mathbf{v} - \pi_2)'\mathbf{\Sigma_2}(\mathbf{v} - \pi_2). \tag{11}$$

2.3 Support Vector Machines with Linear Kernels

Linear discriminant functions define decision hypersurfaces or hyperplanes in a multidimensional feature space:

$$g(\mathbf{v}) = \mathbf{w}^T\mathbf{v} + w_0 = 0 \tag{12}$$

where $\mathbf{w}$ is the weight vector and w_0 is the threshold. $\mathbf{w}$ is orthogonal to the decision hyperplane. The goal is to find the unknown parameters $w_i, i = 1, ..., N$ which define the decision hyperplane [13].

Let $\mathbf{v}_i$, $i = 1, 2, ..., l$ be the feature vectors of the training set. These belong to two different classes, ω_1 or ω_2. If the classes are linearly separable, the objective is to design a hyperplane that classifies correctly all the training vectors. This hyperplane is not unique and it can be estimated maximizing the performance of the classifier, that is, the ability of the classifier to operate satisfactorily with new data. The maximal margin of separation between both classes is a useful design criterion. Since the distance from a point $\mathbf{v}$ to the hyperplane is given by $z = |g(\mathbf{x})|/ \parallel \mathbf{w} \parallel$, the optimization problem can be reduced to the maximization of the margin $2/ \parallel \mathbf{w} \parallel$ with constraints by scaling $\mathbf{w}$ and w_0 so that the value of $g(\mathbf{v})$ is $+1$ for the nearest point in w_1 and -1 for the nearest point in w_2. The constraints are the following:

$$\mathbf{w}^T\mathbf{v} + w_0 \geq 1, \forall \mathbf{v} \in w_1 \tag{13}$$

$$\mathbf{w}^T\mathbf{v} + w_0 \leq 1, \forall \mathbf{v} \in w_2, \tag{14}$$

or, equivalently, minimizing the cost function $J(\mathbf{w}) = 1/2\|\mathbf{w}\|^2$ subject to:

$$y_i(\mathbf{w}^T\mathbf{x}_i + w_0) \geq 1, i = 1, 2, ..., l. \tag{15}$$

2.4 k-Nearest-Neighbor

An object is classified by a majority vote of its neighbors, with the object being assigned to the most common class amongst its k nearest neighbors. k is a positive integer, typically small. For instance, if $k = 1$, then the object is simply assigned to the class of its nearest neighbor. We choose $k = 3$ and euclidean distance in the experimental results.

3 SPECT Image Acquisition and Preprocessing

The patients were injected with a gamma emitting ^{99m}Tc-ECD radiopharmaceutical and the SPECT raw data was acquired by a three head gamma camera Picker Prism 3000. A total of 180 projections were taken for each patient with a 2-degree angular resolution. The images of the brain cross sections were reconstructed from the projection data using the filtered backprojection (FBP) algorithm in combination with a Butterworth noise removal filter [14].

The complexity of brain structures and the differences between brains of different subjects make necessary the normalization of the images with respect to a common template. This ensures that the voxels in different images refer to the same anatomical positions in the brain. In this work, the images have been normalized using a general affine model, with 12 parameters [15, 16].

After the affine normalization, the resulting image is registered using a more complex non-rigid spatial transformation model. The deformations are parameterized by a linear combination of the lowest-frequency components of the three-dimensional cosine transform bases [17]. A small-deformation approach is used, and regularization is by the bending energy of the displacement field. Then, we normalize the intensities of the SPECT images with respect to the maximum intensity, which is computed for each image individually by averaging over the 3% of the highest voxel intensities, similar as in [18].

4 First and Second-Order Moments of SPECT Images

4.1 Mean Image

Firstly, we study the mean intensity values of the Normals and ATD images. Let the brain image set be $I_1, I_2, ..., I_N$, where the number of images N is the sum of the images previously labelled as Normals (N_{NOR}) and Alzheimer type dementia (N_{ATD}) by expertises. The average Normal brain image of the dataset is defined as

$$\bar{I}_{NOR} = \frac{1}{N_{NOR}} \sum_{j \in NOR}^{N_{NOR}} I_j. \tag{16}$$

The average ATD can be calculated analogously:

$$\bar{I}_{ATD} = \frac{1}{N_{ATD}} \sum_{j \in ATD}^{N_{ATD}} I_j. \tag{17}$$

The difference between the mean normal image and the mean ATD is depicted in Figure 2(a).

In the classification task, we will consider those voxels i which present a difference greater than a given threshold ε_μ.

$$i \quad / \quad \{|\bar{I}_{NOR}(i) - \bar{I}_{ATD}(i)| > \varepsilon_\mu\} \tag{18}$$

Figure 1 shows the distribution of the voxels i with $|\bar{I}_{NOR}(i) - \bar{I}_{ATD}(i)|$ greater than six different threshold values ε_μ. It is easily seen that, if the whole image

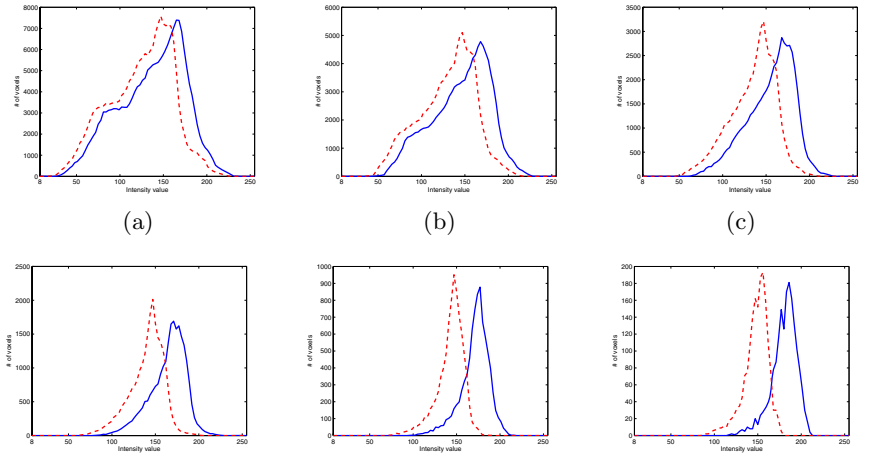

Fig. 1. Histogram with the intensity values of selected voxels with varied ε_μ. Continuous line: mean normal image. Dotted line: mean ATD image. (a) $\varepsilon_\mu = 5$, (b) $\varepsilon_\mu = 10$, (c) $\varepsilon_\mu = 15$, (d) $\varepsilon_\mu = 20$, (e) $\varepsilon_\mu = 25$ and (f) $\varepsilon_\mu = 30$.

is considered, their distributions are quite similar. The difference between the histogram of the mean normal and ATD images increases concomitantly with the threshold value ε_μ.

4.2 Standard Deviation Image

The root-mean-square deviation from their mean for normal images is defined as

$$I^{\sigma}_{NOR} = \sqrt{\frac{1}{N_{NOR}} \sum_{j \in NOR}^{N_{NOR}} (I_j - \overline{I}_{NOR})^2}, \tag{19}$$

and for ATD:

$$I^{\sigma}_{ATD} = \sqrt{\frac{1}{N_{ATD}} \sum_{j \in ATD}^{N_{ATD}} (I_j - \overline{I}_{ATD})^2}. \tag{20}$$

The resulting image $I^{NOR}_{\sigma} + I^{ATD}_{\sigma}$ is plotted in Figure 2(b). This figure help us to discriminate those areas of the brain which present lower dispersion between images.

We propose a criterion to select discriminant voxels by means of the information given by the mean and standard deviation of the images. This procedure consists in select those voxels i which hold the condition in expression (18) for a given threshold value ε_μ and also satisfy the following criterion:

$$i \quad / \quad \{I^{\sigma}_{NOR}(i) + I^{\sigma}_{ATD}(i) < \varepsilon_\sigma\}. \tag{21}$$

the mean of selected voxels will be used as features for the classification task.

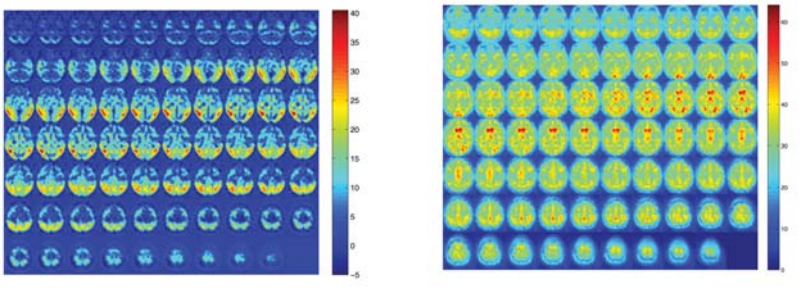

(a) (b)

Fig. 2. (a) Difference between Normal and ATD mean images. (b) Sum of the images I^{σ}_{NOR} and I^{σ}_{ATD}.

5 Results

The performance of the classification is tested on a set of 79 real SPECT images (41 normals and 38 ATD) of a current study using the leave one-out method: the classifier is trained with all but one images of the database. The remaining image, which is not used to define the classifier, is then categorized. In that way, all SPECT images are classified and the success rate is computed from the number of correctly classified subjects.

We consider those voxels which fulfill the condition in equation (18) and also present lower dispersion. We measure the dispersion of the intensity values for normals and ATD images by mean of the standard deviation images I^{σ}_{NOR} and I^{σ}_{ATD}.

We consider voxels which fulfill the condition $|\bar{I}_{NOR}(i) - \bar{I}_{ATD}(i)| > \varepsilon_{\mu}$ with $\varepsilon_{\mu} = 25$ and $\varepsilon_{\mu} = 30$ in addition to the condition $I^{NOR}_{\sigma} + I^{ATD}_{\sigma} < \varepsilon_{\sigma}$ for different threshold values ε_{σ}. In Figure 3, the classification performance versus the threshold value ε_{σ} is plotted. We obtain a classification accuracy greater

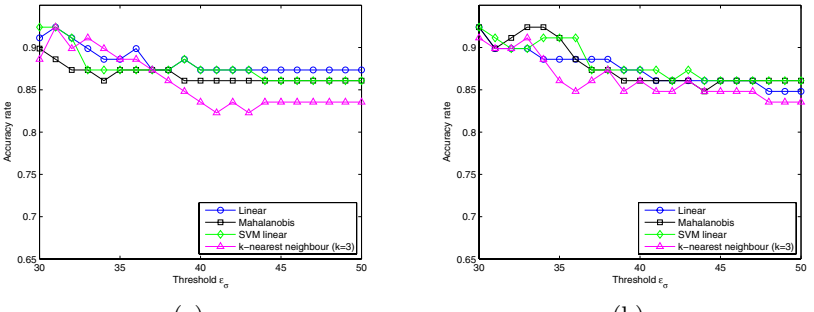

(a) (b)

Fig. 3. Accuracy rate versus threshold value ε_{σ}. Selected voxels fulfill the condition $|\bar{I}_{NOR}(i) - \bar{I}_{ATD}(i)| > \varepsilon_{\mu}$, with threshold: (a) $\varepsilon_{\mu} = 25$, (b) $\varepsilon_{\mu} = 30$.

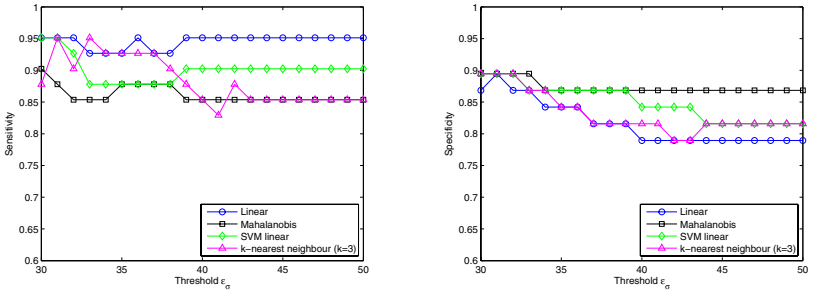

(a) (b)

Fig. 4. Selected voxels fulfill the condition $|\bar{I}_{NOR}(i) - \bar{I}_{ATD}(i)| > \varepsilon_\mu$, with threshold: $\varepsilon_\mu = 25$. (a) Sensitivity versus threshold value ε_σ. (b) Specificity versus ε_σ.

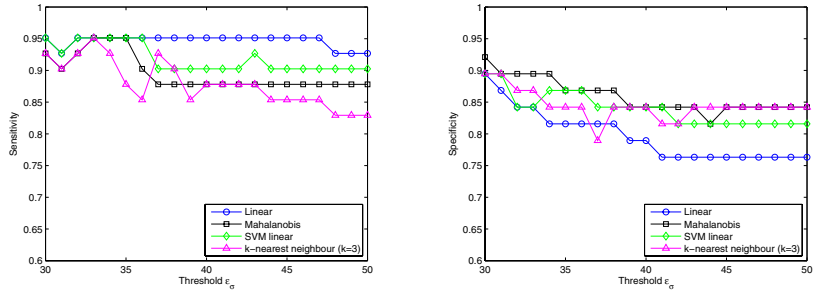

(a) (b)

Fig. 5. Selected voxels fulfill the condition $|\bar{I}_{NOR}(i) - \bar{I}_{ATD}(i)| > \varepsilon_\mu$, with threshold: $\varepsilon_\mu = 30$. (a) Sensitivity versus threshold value ε_σ. (b) Specificity versus ε_σ.

than 92%. Furthermore, the proposed selection of voxels allows us to obtain a high accuracy rate independently of the classifier. For instance, Figures 3(a) and 3(b) show that multivariate normals (linear), and SVM with linear kernel achieve similar performances.

Figures 4 and 5 plot the Sensitivity and Specificity in the classification task versus ε_σ for voxels which fulfill the condition $|\bar{I}_{NOR}(i) - \bar{I}_{ATD}(i)| > \varepsilon_\mu$ with $\varepsilon_\mu = 25$ and $\varepsilon_\mu = 30$ respectively. We obtain a sensitivity of 95% and a specificity of 90% for certain values of the threshold ε_σ.

6 Conclusion

In this work, a straightforward criterion to select a set of discriminant voxels for the classification of SPECT brain images is presented. After normalisation of the brain images, the set of voxels which presents greater overall difference between normals and Alzheimer type dementia images and also lower dispersion is selected. The mean value of the selected voxels are used as features to different

classifiers. The classification accuracy was 92%. The method proposed in this work allows us to classify the brain images in normal and affected subjects with no prior knowledge about the Alzheimer disease.

Acknowledgment

This work was partly supported by the Spanish Government under the PETRI DENCLASES (PET2006-0253), TEC2008-02113, NAPOLEON (TEC2007-68030-C02-01) projects and the Consejera de Innovación, Ciencia y Empresa (Junta de Andaluca, Spain) under the Excellence Project (TIC-02566).

References

[1] English, R.J., Childs, J. (eds.): SPECT: Single-Photon Emission Computed Tomography: A Primer. Society of Nuclear Medicine (1996)

[2] Hellman, R.S., Tikofsky, R.S., Collier, B.D., Hoffmann, R.G., Palmer, D.W., Glatt, S., Antuono, P.G., Isitman, A.T., Papke, R.A.: Alzheimer disease: quantitative analysis of I-123-iodoamphetamine SPECT brain imaging. Radiology 172, 183–188 (1989)

[3] Holman, B.L., Johnson, K.A., Gerada, B., Carvalho, P.A., Satlin, A.: The scintigraphic appearance of alzheimer's disease: A prospective study using Technetium-99m-HMPAO SPECT. Journal of Nuclear Medicine 33(2), 181–185 (1992)

[4] Johnson, K.A., Kijewski, M.F., Becker, J.A., Garada, B., Satlin, A., Holman, B.L.: Quantitative brain SPECT in Alzheimer's disease and normal aging. Journal of Nuclear Medicine 34(11), 2044–2048 (1993)

[5] Jagust, W., Thisted, R., Devous, M.D., Heertum, R.V., Mayberg, H., Jobst, K., Smith, A.D., Borys, N.: Spect perfusion imaging in the diagnosis of alzheimer's disease: A clinical-pathologic study. Neurology 56, 950–956 (2001)

[6] McNeill, R., Sare, G.M., Manoharan, M., Testa, H.J., Mann, D.M.A., Neary, D., Snowden, J.S., Varma, A.R.: Accuracy of single-photon emission computed tomography in differentiating frontotemporal dementia from alzheimer's disease. J. Neurol. Neurosurg. Psychiatry 78(4), 350–355 (2007)

[7] Ramírez, J., Górriz, J.M., Romero, A., Lassl, A., Salas-Gonzalez, D., López, M., Gómez-Río, M., Rodríguez, A.: Computer aided diagnosis of alzheimer type dementia combining support vector machines and discriminant set of features. Information Sciences (2008) (accepted)

[8] Fung, G., Stoeckel, J.: SVM feature selection for classification of SPECT images of Alzheimer's disease using spatial information. Knowledge and Information Systems 11(2), 243–258 (2007)

[9] Górriz, J.M., Ramírez, J., Lassl, A., Salas-Gonzalez, D., Lang, E.W., Puntonet, C.G., Álvarez, I., López, M., Gómez-Río, M.: Automatic computer aided diagnosis tool using component-based svm. In: Medical Imaging Conference, Dresden. IEEE, Los Alamitos (2008)

[10] Lassl, A., Górriz, J.M., Ramírez, J., Salas-Gonzalez, D., Puntonet, C.G., Lang, E.W.: Clustering approach for the classification of spect images. In: Medical Imaging Conference, Dresden. IEEE, Los Alamitos (2008)

[11] Stoeckel, J., Malandain, G., Migneco, O., Koulibaly, P.M., Robert, P., Ayache, N., Darcourt, J.: Classification of SPECT images of normal subjects versus images of Alzheimer's disease patients. In: Niessen, W.J., Viergever, M.A. (eds.) MICCAI 2001. LNCS, vol. 2208, pp. 666–674. Springer, Heidelberg (2001)
[12] Krzanowski, W.J. (ed.): Principles of multivariate analysis: a user's perspective. Oxford University Press, Inc., New York (1988)
[13] Vapnik, V.: Statistical learning theory. John Wiley and Sons, New York (1998)
[14] Ramírez, J., Górriz, J.M., Gómez-Río, M., Romero, A., Chaves, R., Lassl, A., Rodríguez, A., Puntonet, C.G., Theis, F., Lang, E.: Effective emission tomography image reconstruction algorithms for spect data. In: Bubak, M., van Albada, G.D., Dongarra, J., Sloot, P.M.A. (eds.) ICCS 2008, Part I. LNCS, vol. 5101, pp. 741–748. Springer, Heidelberg (2008)
[15] Salas-Gonzalez, D., Górriz, J.M., Ramírez, J., Lassl, A., Puntonet, C.G.: Improved gauss-newton optimization methods in affine registration of spect brain images. IET Electronics Letters 44(22), 1291–1292 (2008)
[16] Woods, R.P., Grafton, S.T., Holmes, C.J., Cherry, S.R., Mazziotta, J.C.: Automated image registration: I. general methods and intrasubject, intramodality validation. Journal of Computer Assisted Tomography 22(1), 139–152 (1998)
[17] Ashburner, J., Friston, K.J.: Nonlinear spatial normalization using basis functions. Human Brain Mapping 7(4), 254–266 (1999)
[18] Saxena, P., Pavel, D.G., Quintana, J.C., Horwitz, B.: An automatic threshold-based scaling method for enhancing the usefulness of Tc-HMPAO SPECT in the diagnosis of Alzheimer's disease. In: Wells, W.M., Colchester, A.C.F., Delp, S.L. (eds.) MICCAI 1998. LNCS, vol. 1496, pp. 623–630. Springer, Heidelberg (1998)